Appl. Phys. B 70, 627–633 (2000) / Digital Object Identifier (DOI) 10.1007/s003409900172

Applied Physics B
Lasers
and Optics

Quantitative wavelength-modulation spectroscopy without certified gas mixtures

J. Henningsen*, **H. Simonsen**

Danish Institute of Fundamental Metrology Bld.307, Anker Engelunds Vej 1, DK 2800 Lyngby, Denmark
(Fax: +45-45/931-137, E-mail: jh@dfm.dtu.dk; hs@dfm.dtu.dk)

Received: 20 August 1999/Revised version: 2 September 1999/Published online: 30 November 1999

Abstract. We study the quantification of signal strength in wavelength-modulation spectroscopy, and present algorithms which allow for the quantitative analysis of second-harmonic spectra for arbitrary combinations of line width and modulation depth. The algorithms are validated through measurements on CO lines in the $0 \rightarrow 3$ overtone band. They can be used for measuring the line strength of lines that are too weak to allow direct absorbance measurements, and for quantifying the response from monitors applying wavelength-modulation under conditions where calibration with certified gases is not feasible.

PACS: 33.70.Fd; 42.68.Ca; 42.68.Wt

The detection of trace amounts of specific molecules in an unspecified gaseous matrix is one of the fundamental problems in environmental science. One widely used technique relies on the fact that many molecules have a highly characteristic infrared absorption spectrum which produces what is often referred to as a fingerprint of the molecule. If the spectrum is known from laboratory studies, a measurement of the absorption coefficient in one or several suitable lines will in principle yield not only the concentration of the molecules, but also an unambiguous identification. For practical applications the use of room-temperature near-infrared diode lasers addressing molecular overtone or combination bands has gained increasing importance over the last decade [1, 2]. In this work we shall focus on the implementation of this technique through wavelength-modulation spectroscopy (WMS) and second-harmonic detection (2f).

WMS is the earliest implementation of modulation spectroscopy [3], where the laser wavelength is modulated at a relatively low frequency in the kHz range, and the response is recorded at the n^{th} harmonic of the modulation frequency. If the modulation amplitude is much smaller than the line width, the reponse is proportional to the n^{th} derivative of the absorbance, and this technique is therefore also referred to as derivative spectroscopy. Although modulation of wavelength and frequency is obviously the same thing, it has become customary to talk about frequency modulation if the modulation frequency is so high that the individual side bands are resolved [4]. Different schemes using one- or two-tone frequency modulation in the MHz to GHz range lead to a reduction in laser noise, and consequently to increased sensitivity in applications where laser noise is the limiting factor. However, in practical monitoring this is rarely the case [5], and since WMS is technically simpler, it will often represent the best choice. A second reason for retaining interest in WMS is the recent commercial availability of extended-cavity diode laser systems which can be grating-tuned single-mode over a wide range, and which are therefore ideal sources for spectroscopy. These lasers are wavelength-modulated by controlling the cavity length with a piezoelectric element, and for this reason the modulation frequency is limited to the low-kHz range.

In the weak-modulation limit of WMS the second-harmonic response can be related in a precise way to the second derivative of the absorbance, and hence to the trace gas concentration, if the absorption path length is known. However, in order to maximise the signal-to-noise ratio, a modulation amplitude is required that is far beyond this limit, so that the modulation itself strongly affects the line profile. The conventional way of obtaining quantitative information would then be to compare the measured response to that generated by a calibration gas with known content of the molecule in question. However, this method is not always feasible. First of all, it requires access to calibration mixtures which may be expensive, and which have a limited lifetime. Moreover, certain molecules are reactive or short-lived so that it is just not possible to make and maintain mixtures with well-defined concentrations. Finally, in practical monitoring, the introduction of a calibration gas in the measurement volume may be technically difficult or even impossible. This is for example the case when monitoring combustion or other processes where the molecules are subject to conditions far from ambient. In the following we shall discuss the problem of quantifying the measured response and provide tools which will allow the deduction of the concentration directly from the second-harmonic response in conjunction with the

*Corresponding author.

molecular parameters, the characteristics of the laser, and the parameters that characterise the experimental conditions.

1 Line-shape analysis

Radiation travelling over a path length L in a medium with absorption coefficient α suffers an exponential intensity loss $\exp(-\gamma)$ where $\gamma = \alpha L$ denotes the absorbance. In the vicinity of an absorption line centred at frequency ν_0, the absorbance is given by

$$\gamma = L\,NSg\,(\nu - \nu_0)\ , \tag{1}$$

where N is the number density of absorbing molecules, S is the strength of the absorption line, and $g(\nu - \nu_0)$ is the area-normalised line-shape function. The power reaching the detector is given by

$$P = P_0\kappa\exp(-\gamma) \simeq P_0\kappa(1-\gamma)\ , \tag{2}$$

where P_0 is the power launched into the absorption path, the factor κ accounts for all losses except those associated with the absorption line, and the expansion holds in the limit of weak absorption where $\gamma \ll 1$.

1.1 Pure frequency modulation

The laser frequency ν is modulated according to $\nu(t) = \nu + \nu_m \sin(\omega_m t)$, and the response is detected with a lock-in amplifier. Using 2f demodulation, the lock-in detector will recover the rms value of the second-harmonic Fourier component. Assuming pure frequency modulation and linear detection, and assuming that only the term containing γ is modulated, we find that the lock-in output, normalised with respect to the dc detector voltage, can be written as

$$u_{2h} = \frac{-1}{\sqrt{2}} L\,NSg_{2h}\ , \tag{3}$$

where

$$g_{2h} = \frac{1}{\pi}\int_0^{2\pi} g\,(\nu + \nu_m \sin(\omega_m t) - \nu_0)\cos(2\omega_m t)\mathrm{d}\,(\omega_m t)\ . \tag{4}$$

In the weak-modulation limit where the modulation amplitude ν_m is much smaller than the line width, the line-shape function can be Taylor-expanded as

$$\begin{aligned} g(\nu - \nu_0 + \nu_m \sin(\omega_m t)) \simeq\ & g\,(\nu - \nu_0) \\ & + g'\,(\nu - \nu_0)\,\nu_m \sin(\omega_m t) \\ & + \frac{1}{4} g''\,(\nu - \nu_0)\,\nu_m^2\,(1 - \cos(2\omega_m t)) + \ldots\ , \end{aligned} \tag{5}$$

and we find the usual result that the second-harmonic signal

$$u_{2h} \simeq \frac{1}{4\sqrt{2}} L\,NS\nu_m^2 g''\,(\nu - \nu_0) \tag{6}$$

is proportional to the second derivative of the line-shape function. If the weak modulation condition is not fulfilled, the integral in (4) must be evaluated numerically, and we must be concerned with the functional behaviour of the line-shape. To a very good approximation the line-shape will be given by a Voigt function, which is the convolution of a Doppler profile characterised by a Doppler width $\Delta\nu_\mathrm{D}$ and a Lorentz function characterised by a collisional width $\Delta\nu_\mathrm{L}$, both referring to half width at half maximum (HWHM). The width $\Delta\nu$ of the Voigt profile cannot be expressed analytically, but for the present purpose we shall use the approximation

$$\Delta\nu = \left(\Delta\nu_\mathrm{D}^2 + \Delta\nu_\mathrm{L}^2\right)^{1/2}\ . \tag{7}$$

We define the modulation depth $b \equiv \nu_m/\Delta\nu$. In the weak-modulation limit $b \ll 1$, the second-harmonic signal is quadratic in b and proportional to the second derivative of the absorbance. For a Voigt profile with a HWHM line width of 1 GHz, Fig. 1 shows the change of the profile as the modulation amplitude is gradually increased through the sequence $b = 0.2, 0.5, 1, 2, 5$.

To characterise the second-harmonic line-shape function g_{2h} we introduce the amplitudes g_1 and g_2 and the apparent width $\Delta\nu_\mathrm{app}$ as indicated in Fig. 1. By evaluating (4) for a range of values $0.1 < \nu_m < 12.5$ GHz and $0.5 < \Delta\nu < 2.5$ GHz, with a constant Doppler contribution of 0.2 GHz, we find that the three quantities can be expressed as functions of the modulation depth b in the following way:

$$(g_1 + g_2)\pi\Delta\nu = F(b)\ , \tag{8}$$

$$g_2/g_1 = G(b)\ , \tag{9}$$

$$\Delta\nu_\mathrm{app}/\Delta\nu = H(b)\ . \tag{10}$$

The calculated values are shown in Fig. 2 together with full lines which represent the interpolation formulae

$$F(b) = 1.02\frac{-0.52b^{0.12} + 1}{0.55b^{0.12} + b^{-2}}\ , \tag{11}$$

$$G(b) = \frac{0.30b^{1.656} + 4}{0.47b^{1.656} + 1}\ , \tag{12}$$

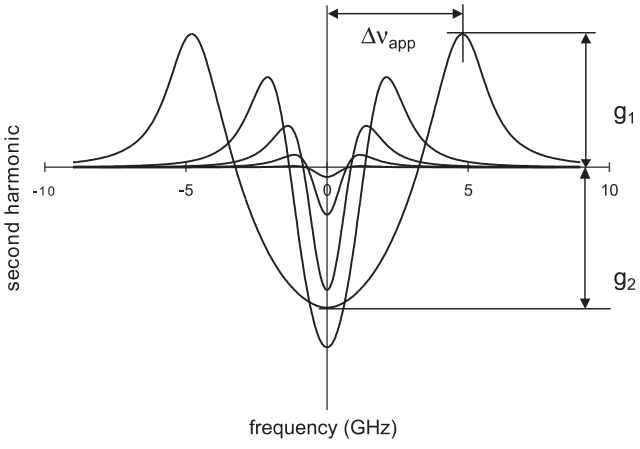

Fig. 1. Broadening of the second-harmonic profile for a line with 1-GHz HWHM line width with increasing modulation depth b (= 0.2, 0.5, 1, 2, 5). The profile is characterised by the amplitudes g_1 and g_2, and by the apparent width $\Delta\nu_\mathrm{app}$

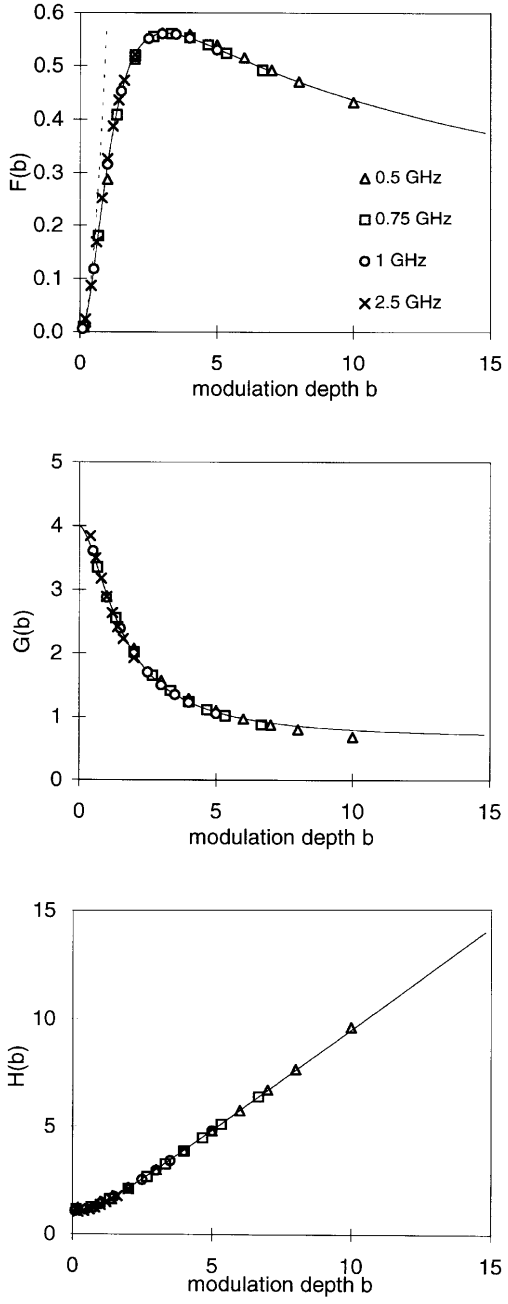

Fig. 2. Functions *F(b)*, *G(b)*, and *H(b)*, characterising a strongly modulated Voigt profile. Different symbols refer to different HWHM line widths for a fixed Doppler width of 0.2 GHz. *Solid lines* represent model functions, and the *dotted curve* in *F(b)* represents the analytical limit for $b \to 0$

$$H(b) = \left(0.89b^2 + 1\right)^{1/2} . \tag{13}$$

The functional form of the interpolation formulae were chosen by trial so as to provide a qualitatively correct representation of the calculated data points, and the numerical constants were subsequently determined by least-square fits, providing good quantitative agreement over the range $0.1 < b < 10$. The dotted curve on the graph for *F(b)* represents the Taylor expansion limit (6) where the second derivative is evaluated in the Lorentz limit. It is clearly seen that this approximation fails long before the signal has reached its maximum value. For $G(b)$ and $H(b)$ the Taylor expansion in the Lorentz limit implies $G(b \to 0) = 4$ and $H(b \to 0) = 1$, and the model functions are chosen such that they provide these limiting values.

Unfortunately, it is not customary in spectroscopy to use SI units consistently. In the following we therefore use the units that are conventionally applied, and give expressions which relate the measured signals to the concentration of absorbing molecules, including the conversion factors needed in order to connect the different units. Using the ideal gas law we can express the number density N as

$$N = c\frac{p}{kT} , \tag{14}$$

where c is the concentration, p the pressure, and T the temperature. For the peak absorbance we then get from (1)

$$\gamma(0) = 2.171 \times 10^{20} \times c\,[\mathrm{mol/mol}]\, L\,[\mathrm{m}]\, \frac{p\,[\mathrm{Pa}]}{T\,[\mathrm{K}]} S\,[\mathrm{cm/mol}] \times g_{\mathrm{V}}(0)\left[\mathrm{GHz}^{-1}\right] , \tag{15}$$

where the concentration c is expressed in dimensionless form as [mol/mol], and where $g_{\mathrm{V}}(0)$ is the maximum value of the area-normalised Voigt function. The numerical factor is derived as

$$2.171 \times 10^{20} = 100\,[\mathrm{cm/m}]\, \frac{10^{-6}\,[\mathrm{cm}^{-3}/\mathrm{m}^{-3}]}{1.3806 \times 10^{-23}\,[\mathrm{J/K}]} \times 29.979\,[\mathrm{GHz/cm}^{-1}] . \tag{16}$$

Using this result together with (3) and (8), we find for the peak-to-peak amplitude of the second-harmonic signal

$$u_{\mathrm{pp}} = 2.171 \times 10^{20} \times c\,[\mathrm{mol/mol}]\, L\,[\mathrm{m}]\, \frac{p\,[\mathrm{Pa}]}{T\,[\mathrm{K}]} S\,[\mathrm{cm/mol}] \times \frac{F(b)}{\sqrt{2}\pi\,\Delta\nu\,[\mathrm{GHz}]} . \tag{17}$$

In the Lorentz limit, which is an excellent approximation at ambient pressure, we have

$$g_{\mathrm{V}}(0) \to g_{\mathrm{L}}(0) = \frac{1}{\pi\,\Delta\nu_{\mathrm{L}}} , \tag{18}$$

and introducing this in (15), we can relate the second-harmonic peak-to-peak amplitude u_{pp} to the peak absorbance as

$$u_{\mathrm{pp}} = \gamma(0)\frac{F(b)}{\sqrt{2}} . \tag{19}$$

1.2 Mixed wavelength and amplitude modulation

Whereas the assumption of pure wavelength-modulation is fairly good for a well-behaved extended-cavity diode laser modulated by changing the length of the resonator, a DFB laser modulated through the injection current will always experience simultaneous wavelength and amplitude modulation. If the power depends linearly on the injection current,

this can be accounted for by introducing an additional amplitude modulation factor in (4)

$$g_{2h} = \frac{1}{\pi}\int_0^{2\pi} (1+\alpha_m \sin(\omega_m t))\, g\,(\nu + \nu_m \sin(\omega_m t) - \nu_0) \times \cos(2\omega_m t)\mathrm{d}(\omega_m t) \ . \quad (20)$$

In general one would have to allow for a phase difference between the modulation of frequency and amplitude, but for the low modulation frequencies typical of WMS this may be disregarded. Also, since both terms in (2) are modulated, normalisation of the second-harmonic signal should be performed with respect to the detector signal averaged over the modulation cycle. In the weak modulation limit $\alpha_m \ll 1$ and $b \ll 1$, amplitude modulation leads to an additional second-harmonic contribution which is proportional to the first derivative of the line-shape function:

$$g_{2h,a} = \frac{1}{2}\alpha_m \nu_m g'\,(\nu - \nu_0) \ . \quad (21)$$

The main effect of this term is to introduce an asymmetry with respect to the line centre as shown in Fig. 3. Since the term induced by the amplitude modulation is antisymmetric with respect to the line centre, the quantity g_1 entering in the definitions of $F(b)$ (8) and $G(b)$ (9) can be taken as the mean value of the maxima on the low- and high-frequency side of the line centre. The two maxima will be slightly displaced towards the line centre, but to a good approximation this effect can be neglected, and we can determine the apparent line width from the measured positions of the maxima.

If the weak modulation limit does not apply, the integral in (20) must be evaluated numerically, and we find that the conclusions for weak modulation remain valid. This also follows from the fact that the amplitude modulation term remains antisymmetric with respect to the line centre to all orders in a Taylor expansion. The lower graph of Fig. 3 shows the variation of laser power with increasing injection current, corresponding to decreasing frequency. Since an increase in injection current will increase the power and decrease the frequency, it follows from (20) that α_m and ν_m have opposite signs.

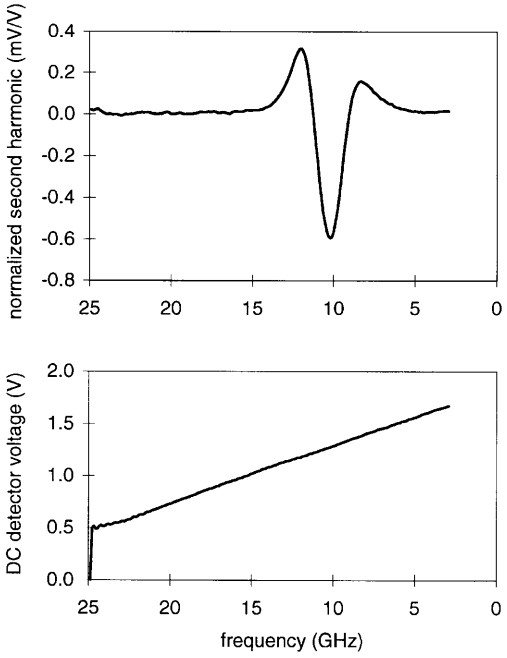

Fig. 3. Line asymmetry induced in the second-harmonic profile by simultaneous amplitude and wavelength-modulation

2 Experiments

The expressions for $F(b)$, $G(b)$, and $H(b)$ were validated with the experimental arrangement shown in Fig. 4. Radiation from an extended-cavity laser (New Focus Model 6262) passes through a 30-dB bulk isolator and through a pellicle beam splitter (Edmund Scientific) which directs about 10% of the radiation to an air-spaced Fabry–Pérot etalon with 2 GHz free spectral range (Tec Optics). The remaining 90% is transmitted through the 15-cm absorption cell and is then detected by a 5×5 mm Ge photo diode (Judson J16). The laser can be tuned over 70 nm by rotating the grating of the extended cavity with a motor, and for fixed setting of the grating, the frequency can be fine tuned over 30 GHz by scanning a bias voltage which controls the length of the resonator through a piezoelectric element.

A modulation voltage at 313 Hz was superimposed on the ramp voltage, and the second-harmonic response was measured with a lock-in amplifier (Stanford Research SR530) using 2 f demodulation. The signal from the photo detector, the second-harmonic output from the lock-in, and the signal transmitted through the Fabry–Pérot etalon, were logged by an AD/DA card (Data Translation DT2802). The 2f performance of the lock-in was checked by means of a linear ramp with a repetition rate of 313 Hz, generated by a high-quality function generator (Stanford Research DS345). The measured second-harmonic signal agreed within 1% with the value calculated from a Fourier analysis of the input.

2.1 Tuning characteristics of the laser

For quantitative analysis of the second-harmonic signal it is crucial that the frequency-tuning behaviour of the laser is accurately known. For this purpose we use the Fabry–Pérot etalon in a scanning mode, and measure the excursions of the resonances as a function of the applied modulation voltage. The upper graph of Fig. 5 shows the rms frequency modulation as a function of the applied rms modulation voltage at 313 Hz, with the piezo biased at 50% of the maximum voltage, while the lower graph shows the rms frequency modulation as a function of piezo bias for a fixed modulation voltage of 0.1 V rms. The sharp decline above 95% is caused by the piezo being overloaded during part of the modulation cycle. We find that that for fixed modulation voltage the frequency modulation coefficient increases from 3.4 GHz/V to 4.6 GHz/V as the bias voltage is increased from 0 to 100%. This reflects the non-linearity of the piezo, and means that a sinusoidal modulation voltage will lead to a slightly non-sinusoidal frequency modulation. In the experiments, we position the line centre close to 50% bias voltage, and in the data analysis we use the frequency modulation coefficient

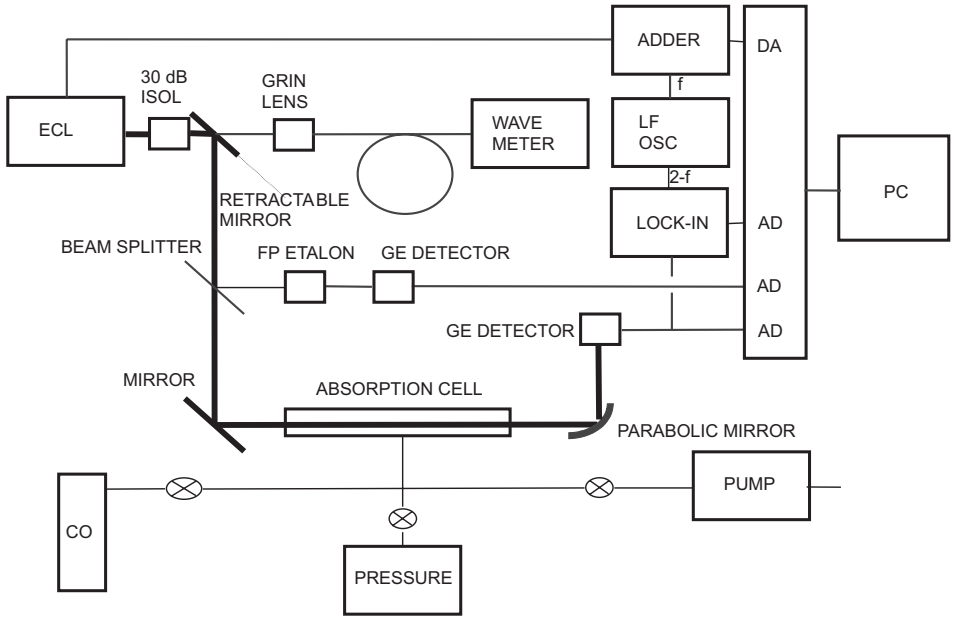

Fig. 4. Experimental arrangement with extended-cavity diode laser (ECL)

4.38 GHz/V corresponding to this situation, neglecting deviations from sinusoidal modulation.

The static-tuning behaviour of the piezo leads to a nonlinearity of the frequency axis which must be accounted for in the data analysis. This is done by switching off the modulation and recording a scan with the Fabry–Pérot etalon in the non-scanning mode. Over the 30-GHz scan range the signal transmitted through the etalon will produce from 14 to 16 transmission spikes separated by the 2.019-GHz free spectral range. A smooth function giving the frequency as a function of step number is generated by cubic spline interpolation between the transmission spikes, and the inverse function is used for evaluating the transmitted signal as a function of frequency in 200 equidistant frequency steps. Further details about the data analysis are given in [6].

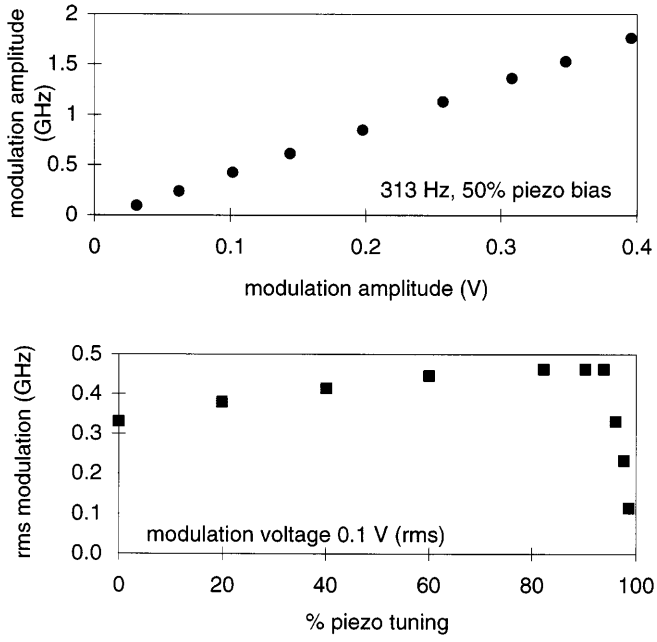

Fig. 5. Modulation characteristics of extended-cavity diode laser

2.2 *Results for* CO

According to (17) the product of the concentration c and the line strength S can be determined from the experiment, provided the pressure p, the temperature T, and the absorption path length L is known. For $c = 1$ this allows determination of the line strength, whereas in the context of monitoring a knowledge of the line strength allows determination of the concentration c. In order to avoid introducing uncertainty from the concentration, we have chosen to work with pure gas, so that $c = 1$, and base the validation of the algorithms on a comparison of the line strength determined from the experiment with the literature value.

Carbon monoxide of nominal purity 99.998% was supplied to the cell, and the line width was varied by controlling the pressure, which was measured with an absolute pressure gauge (Baltzer TPG10). We used the line R7 at 1568.0355 nm with a line strength of $S = 2.179 \times 10^{-23}$ cm/mol and a pressure broadening parameter of $\Delta\nu_L$ = 1.942 MHz/mbar [6]. Measurements were performed at a temperature of 296.5 K and at pressures of 300 mbar and 999 mbar, and in conjunction with a Doppler width of 0.222 GHz we find a combined line width of 0.623 GHz at 300 mbar and 1.953 GHz at 999 mbar according to (7). Under these conditions the peak absorbance is less than 4%, and the condition implied in (2) is well satisfied. Before initiating a scan, the Fabry–Pérot etalon was used in a scanning mode for verifying single-mode operation. The grating angle was chosen such that the line was positioned near the centre of the fine-tuning window, and the piezo voltage was ramped in 1000 steps from 0 to 100%.

With modulation amplitudes in the range 0.43 GHz $< \nu_m <$ 2.48 GHz we cover modulation depths in the range $0.2 < b < 4$. The measured second-harmonic signals are normalised with respect to the dc level, and from the normalised

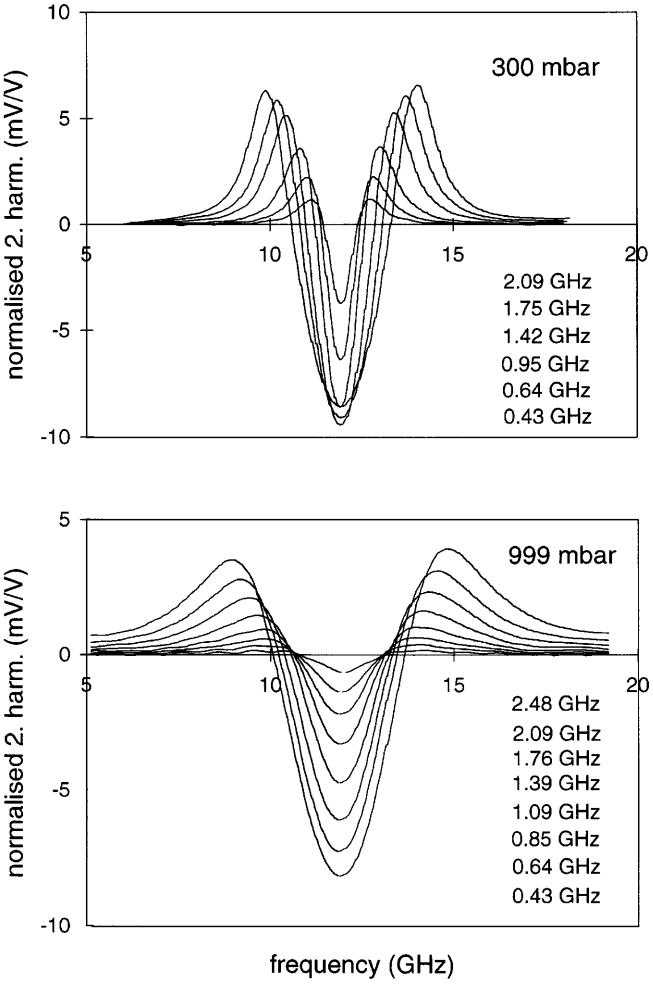

Fig. 6. Experimental normalised second-harmonic amplitudes for different combinations of modulation amplitude and line width (0.623 GHz at 300 mbar and 1.953 GHz at 999 mbar)

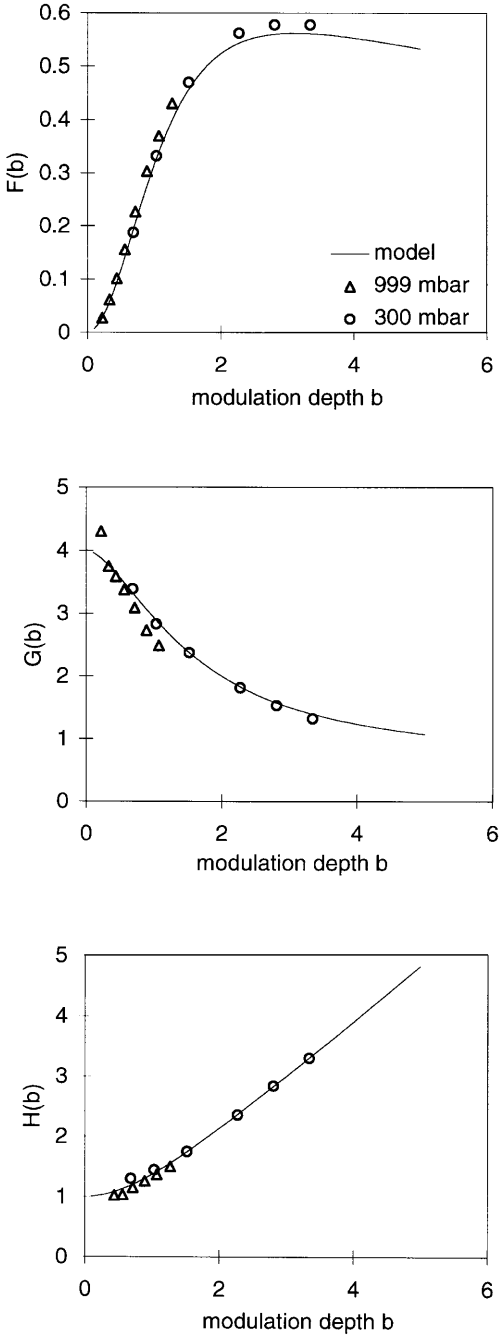

Fig. 7. Experimental values for *F(b)*, *G(b)*, and *H(b)*, compared with the model functions. *Circles* refer to 300 mbar and *triangles* to 999 mbar

signals shown in Fig. 6 together with (17) we may now derive experimental results for *F(b)*, *G(b)*, and *H(b)* to be compared with the model functions (11), (12) and (13). The results are shown in Fig. 7.

The agreement is within 3% for all three functions for 300 mbar and within 8% for 999 mbar.

In order to assess how the deviations will affect the analysis, the data of Fig. 6 are used for deriving the line strength and the line width of R7. As a first step in the analysis, the apparent line width $\Delta\nu_{\mathrm{app}}$ is read from the spectra, and from $H(b)$ and the definition of b the line width is found as

$$\Delta\nu = \sqrt{\Delta\nu_{\mathrm{app}}^2 - 0.89\,\nu_{\mathrm{m}}^2}\,. \tag{22}$$

Next, $F(b)$ is evaluated from (11), and the line strength S may now be determined from (17) with the concentration $c = 1$. The results are given in Fig. 8 and Fig. 9. Comparing with the value quoted by [6] we find that the 300-mbar data produce a mean value that is 6% too high, with most of the discrepancy caused by the two lowest modulation depths. For the 999-mbar data the mean value agrees within the stated 1% standard uncertainty of [6]. For the line width the mean value of the 300-mbar data is too high by 2.4%, whereas the 999 data yield a value that is too low by 7.6%.

The deviations may be attributed to a combination of effects. The scatter of the results seems to increase for low values of the modulation depth where *F(b)* varies rapidly with *b*, and where consequently an uncertainty in the modulation amplitude has a relatively large effect. Furthermore, the analysis is based on assumptions that are not all rigorously satisfied. As seen in Fig. 5 the modulation coefficient expressing the proportionality between applied modulation voltage and the resulting frequency modulation varies during the scan, and for large modulation amplitude there will also

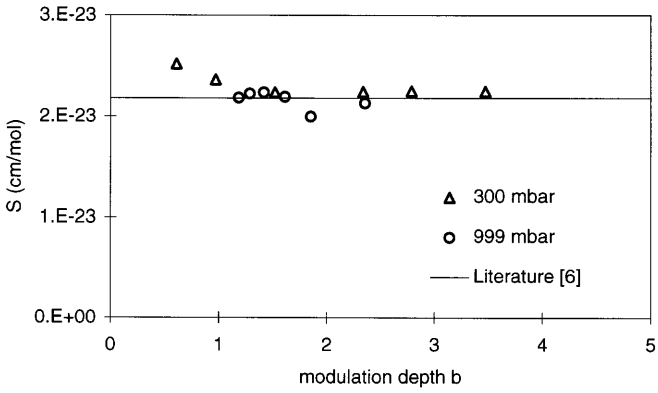

Fig. 8. Line strength determined from 2f spectrum. *Solid line* from literature

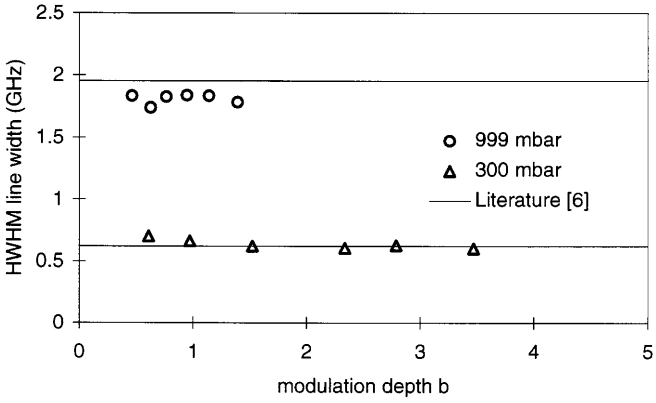

Fig. 9. Line width determined from 2f spectrum. *Solid line* from literature

be a variation during the modulation cycle, leading to a non-sinusoidal modulation.

3 Conclusion

We have developed algorithms for analysing the amplitude of second-harmonic spectra obtained in wavelength-modulation spectroscopy. For pure gases the knowledge of pressure, temperature, and path length is sufficient for the determination of line strength and line width in cases where the signal is too small for the direct measurement of absorbance. For gas mixtures the algorithms allow the direct determination of the concentration of absorbing molecules provided the line strength is known. The accuracy obtained by testing the approach on a known line in the $0 \rightarrow 3$ overtone band of CO is better than 10% for a wide range of line widths and modulation depths.

Acknowledgements. This work has been supported by the Danish Science Research Council under grant no. 9600860, by the European Commission under Contract OG. 269/95, and by base funds from the Danish Agency for Development of Trade and Industry

References

1. H.I. Schiff, G.I. Mackay, J. Bechara: "The use of tunable diode laser absorption spectroscopy for atmospheric measurements". In Chemical Analysis Series, Vol. 127 (Wiley, New York 1994)
2. P. Werle: Spectrochimia Acta Part A **54**, 197 (1998)
3. E.D. Hinkley: Appl. Phys. Lett. **16**, 351 (1970)
4. G.C. Bjorklund, M.D. Levenson, W. Lenth, C. Ortiz: Appl. Phys. B **32**, 145 (1983)
5. I. Linnerud, P. Kaspersen, T. Jaeger: Appl. Phys. B **67**, 297 (1998)
6. J. Henningsen, H. Simonsen, T. Møgelberg, E. Trudsø: J. Mol. Spectrosc. **193**, 354 (1999)